Materials Science and Engineering C 57 (2015) 387–396

Contents lists available at ScienceDirect

Materials Science and Engineering C

journal homepage: www.elsevier.com/locate/msec

Disposable urea biosensor based on nanoporous ZnO film fabricated from omissible polymeric substrate

Reza Rahmanian, Sayed Ahmad Mozaffari *, Mohammad Abedi

Thin Layer and Nanotechnology Laboratory, Institute of Chemical Technology, Iranian Research Organization for Science and Technology (IROST), P.O. Box 33535-111, Tehran, Iran

ARTICLE INFO

Article history:
Received 21 May 2015
Received in revised form 24 July 2015
Accepted 4 August 2015
Available online 11 August 2015

Keywords:
Nanoporous ZnO
Disposable urea biosensor
Omissible polymer
Impedimetric assessment

ABSTRACT

In the present study, a facile and simple fabrication method of a semiconductor based urea biosensor was reported via three steps: (i) producing a ZnO–PVA composite film by means of a polymer assisted electrodeposition of zinc oxide (ZnO) on the F-doped SnO_2 conducting glass (FTO) using water soluble polyvinyl alcohol (PVA), (ii) obtaining a nanoporous ZnO film by PVA omission via a subsequent post-treatment by annealing of the ZnO–PVA film, and (iii) preparation of a FTO/ZnO/Urs biosensor by exploiting a nanoporous ZnO film as an efficient and excellent platform area for electrostatic immobilization of urease enzyme (Urs) which was forced by the difference in their isoelectric point (IEP). The characterization techniques focused on the analysis of the ZnO–PVA film surfaces before and after annealing, which had a prominent effect on the porosity of the prepared ZnO film. The surface characterization of the nanostructured ZnO film by a field emission-scanning electron microscopy (FE–SEM), exhibited a film surface area as an effective bio-sensing matrix for enzyme immobilization. The structural characterization and monitoring of the biosensor fabrication was performed using UV–Vis, Fourier Transform Infrared (FT-IR), Raman Spectroscopy, Thermogravimetric Analysis (TGA), Cyclic Voltammetry (CV), and Electrochemical Impedance Spectroscopy (EIS) techniques. The impedimetric results of the FTO/ZnO/Urs biosensor showed a high sensitivity for urea detection within 8.0–110.0 mg dL^{-1} with the limit of detection as 5.0 mg dL^{-1}.

1. Introduction

Urea [$(NH_2)_2CO$], is a final product of protein metabolism in human organism and any accumulation above critical levels must be carefully determined. The normal level of urea in blood serum is from 15 to 40 mg dL^{-1}. A change in urea level in blood and urine can be caused by urinary tract obstruction, renal failure, burns, dehydration, and shock [1].

The assay of urea can be followed by many different techniques as spectrometry [2–4], potentiometry [5–8], conductometry [9–11], coulometry [12] and amperometry [13]. Recently, many attempts have been extensively made to develop urea electrochemical biosensors, due to their inherent advantages such as robustness, easy miniaturization, excellent detection limits, and requirement of very small amounts of analyte [14,15]. Among the electrochemical urea biosensors, urease (Urs) enzyme based potentiometric biosensors are an ordinary method for determination of urea via utilizing the catalyzed hydrolysis of urea [16,17]. Since potentiometric biosensors suffer from the interference effect by K^+ ions [18], therefore, numerous attempts have been made to develop urea determination methods [19].

Electrochemical impedance spectroscopy (EIS), as an authoritative technique for studying electrical and electrochemical interfacial properties of a large variety of systems, is useful to monitor changes in electrical properties arising from bio-recognition events at the surfaces of modified electrodes [20–25].

In addition, the construction of the transducer surface has a significant effect on the biosensor performance and enzyme immobilization strategy [26]. Nanostructured metal oxides have been recently used for the fabrication of the transducer surface of biosensors because of their unique ability to promote electron transfer between electrode/enzyme active sites and enzyme immobilization with excellent stability [14,27]. Zinc oxide (ZnO), as a typical n-type biocompatible metal oxide with high catalytic efficiency and a good electron communication capability, possesses a high isoelectric point (IEP 9) which makes it suitable for the adsorption of proteins with low IEP (e.g., Urs with IEP of 5.9) via the physical adsorption.

Nanostructured ZnO can be prepared using sol–gel [28], electrophoresis [29], RF sputtering [30], hydrothermal [31], and molecular beam epitaxy [32] techniques. Electrochemical deposition of metal oxides as a cost-effective, reliable, and mild physicochemical method has been an important issue in the preparation of nanostructured metal oxides as transducers [27]. Other often cited advantages of electrodeposition include: high deposition rate, easy scale up and preservation, tuning the process parameters, controlling bath conditions (pH, temperature,

* Corresponding author.
E-mail address: mozaffari@irost.ir (S.A. Mozaffari).

http://dx.doi.org/10.1016/j.msec.2015.08.004
0928-4931/

solvent), and ease of controlling electrolyte formula by adding organic additives, which can be incorporated in producing a substrate with controlled structure and thickness.

In this study, polyvinyl alcohol (PVA) $[CH_2CH(OH)]_n$ as an omissible polymer was applied to produce a ZnO nanoporous film. PVA as a polymeric organic additive interacts with ZnO upon the electrodeposition process and strongly influences the ZnO growth to form a mixed film made of ZnO crystals embedded in a polymer matrix template [33]. Finally, PVA was eliminated by a subsequent annealing treatment of the layer. PVA incorporates advantages to the bio-sensing transducer surface by affording a highly porous platform to the biosensor via its elimination.

Herein, we propose the FTO/ZnO/Urs biosensor of urea by taking advantage of a simple controllable film electrodeposition on the disposable F-doped SnO_2 conducting glass (FTO) for fabricating ZnO film as an efficient bio-sensing transducer for improving sensitivity with a minimum loss of enzyme activity. Impedimetric urea measurements were carried out as a promising assessment method by utilizing an FTO/ZnO/Urs electrode serving as a sensing electrode to achieve appropriate analytical performance in terms of sensitivity and reproducibility. The proposed FTO/ZnO/Urs biosensor showed a fast response time of less than 10 s and retained good enzymatic activity for more than three weeks when kept at a temperature of 4 °C when not in use.

2. Experimental

2.1. Materials and apparatus

Urea (ACS reagent 99.9%), Urs (urease enzyme, E.C.3.5.1 from Jack Bean 100 U mg^{-1}), PVA (Alfa aesar, 87%, high molecular weight, MW 88,000–97,000), $ZnCl_2$ (Aldrich, reagent grade), KCl (ACS reagent), and all other chemicals used in this project were of analytical reagent grade and purchased from Sigma Aldrich. The phosphate buffer solution (PBS) 0.1 M with a pH of 7.4 was prepared from K_2HPO_4 and KH_2PO_4. A stock solution of urea was prepared in 0.1 M PBS with a pH of 7.4, and stored at 4 °C. The low concentration standard solutions of urea were freshly prepared before the measurements. A FTO coated conductive glass was purchased from the Dyesol Company. The surface analysis of ZnO film was carried out using a Tescan Mira II FE-SEM. Thermogravimetric analysis (TGA) was performed using a Mettler Toledo TGA 850 instrument. Raman measurements were performed using a Raman spectrometer, Progeny™ (Rigaku Raman Technologies, Wilmington, DE, USA). Voltammetric and impedimetric experiments were performed using a potentiostat/galvanostat (PGSTAT. 302 N, Autolab, Eco-Chemie, The Netherlands). A FTO/ZnO/Urs electrode served as working electrode (surface area = 1.0 cm^2), while Pt and SCE electrodes were used as counter and reference electrodes, respectively. For EIS measurements, a 10 mV peak-to-peak ac amplitude was applied versus SCE; a range of frequencies from 100 kHz to 10 mHz was scanned and the impedances were recorded. The analysis of the EIS data was performed using Zview/Zplot (Scribner Associates, Inc.), based on Macdonald's algorithm (LEVM 7) using a complex non-linear least square (CNLS) approximation method [34]. Pore size distribution was calculated by "Measurement Software" (Nahamin Pardazan Asia Co., Iran).

2.2. Fabrication of FTO/ZnO nanoporous structure by electrodeposition method

The F-doped SnO_2 conducting glass substrates were cleaned under ultrasonic treatment (5 min in acetone, 5 min in alcohol), rinsed abundantly with water, and finally treated for 2 min in a 45% nitric acid solution prior to drying in nitrogen atmosphere. The deposition solutions were prepared with MilliQ quality water and contained 10^{-1} M KCl and 10^{-2} M $ZnCl_2$. For preparation of a good solubilized PVA polymer as electrolyte, 8.0 g L^{-1} PVA was added to the heated solution of 10^{-1} M KCl and 10^{-2} M $ZnCl_2$ under stirring [33]. The electrochemical cell was placed in a thermo-regulated bath and the deposition temperature was kept constant at 80 °C. The solution was bubbled with O_2 gas for 30 min before the deposition experiment was started. The electrochemical experiments were performed potentiostatically in a three electrode electrochemical cell using the substrate as cathode, a Pt sheet and SCE as counter and the reference electrode, respectively. A constant potential of −1.0 V with the deposition time of 165 s was applied between the working and reference electrodes (Fig. 1). PVA has a dramatic effect on ZnO properties, especially in growth strategies with a catalytic effect in the Zn^{2+} reduction [33]. In order to achieve the FTO/ZnO nanoporous structure, PVA was eliminated by a subsequent post-annealing treatment of the ZnO–PVA layer [33,35–37]. The obtained ZnO nanoporous structure is suitable for enzyme immobilization. The amount of 8.0 g L^{-1} of PVA was chosen as an optimum PVA concentration to achieve a nanoporous ZnO film with a uniform structure, whereas using lower and higher concentrations of PVA led to nanostructures with minimum uniform pores distribution and difficulty of PVA elimination, respectively.

3. Results and discussion

3.1. Field emission-scanning electron microscopy (FE-SEM), optical transmission (UV–vis), FTIR, Raman and TGA studies

Schematic 1 briefly clarifies the effect of PVA omission on the preparation of nanoporous ZnO, where the prepared omissible polymeric film was heated several hours at 400 °C in the air to eliminate PVA. For comparison, FE-SEM images of the ZnO films before and after annealing treatment were shown in Fig. 2. Before annealing, the layer became flat and consisted of aggregated elongated grains that formed a dense film (Fig. 2A). The ZnO and PVA cannot be distinguished on the graphs showing the intimate mixing of the two components. We can also declare that the film became more complicated to study by SEM because of the unsteadiness of the PVA polymer included in the film to the electron beam of the SEM microscope and the appearance of cracks during the observation. Fig. 2B illustrates the surface structure of the post-annealed ZnO film by FE-SEM. The FE-SEM image showed that the grain sizes of the ZnO nanostructured film was found to be in the range of 20–60 nm with a mean size of about 40 nm. The particle size distribution histogram of the ZnO nanostructured film was shown in Fig. 2C.

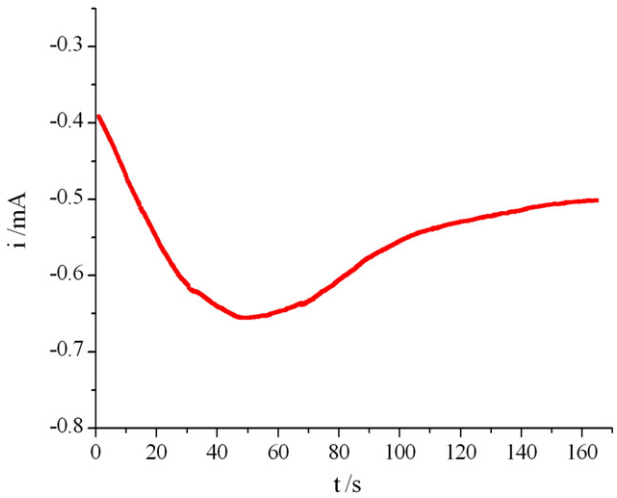

Fig. 1. Chronoamperogram for ZnO–polymer film preparation.

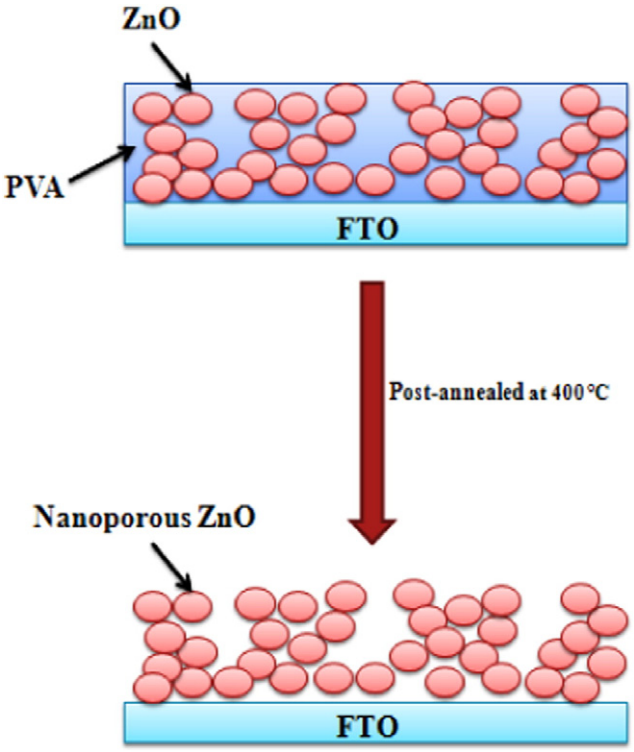

Schematic 1. PVA elimination after annealing for several hours at 400 °C in air in order to fabricate nanoporous ZnO.

The surface analysis of the FE-SEM images of the ZnO film before and after the annealing treatment using "Measurement Software" (Nahamin Pardazan Asia Co.) depicted a distribution pattern and an intensity of pores in quantitative approach and confirmed improvement of surface porosity from 0.09 to 0.45 μm^2 after the annealing treatment, which is believed to play an important role in enzyme immobilization (Fig. 2D and E).

Fig. 2F shows a typical optical transmission (UV–vis) spectrum recorded for the ZnO nanoporous film. The sharp absorption onset and the high transmission values at wavelengths above 338 nm exhibit the optical quality and low concentration of defects such as pits and voids of the ZnO nanoporous film.

The hybrid nature of the films was studied using the FTIR characterization method before and after annealing. The FTIR spectrum of the hybrid film between 400 and 4000 cm^{-1} indicated the characteristics of the ZnO–Polymer nanostructured hybrid film which was prepared with PVA (Fig. 3A). The broad band centered at 3416 cm^{-1} was attributed to the O–H stretching modes of the PVA alcohol groups. This indicated the presence of free exposing –OH groups of the hybrid film. The peak at 2937 cm^{-1} corresponded to stretching vibrations of PVA CH_2 groups [33], while after annealing and PVA elimination, no –OH groups peak and no CH_2 stretching vibration peaks were observed for annealed film (Fig. 3B). Indeed, Raman scattering spectroscopy was employed to study the vibrational properties of the pure ZnO structure after annealing. Fig. 3C shows a typical room-temperature Raman spectrum for the annealed ZnO film in the range of 250–650 cm^{-1}. In the Raman spectra, the ZnO exhibits strong bands at 583, 438, 385, and 331 cm^{-1}, which are corresponding to the $E_1(LO)$, E_2, $A_1(TO)$, and A_1 modes of wurtzite ZnO, respectively [38].

In addition, TGA and differential thermogravimetric analysis (DTG) techniques were applied in the study of PVA as an omissible polymeric substrate. These analytical techniques were utilized to determine ZnO–PVA thermal stability by monitoring the weight loss of the sample as a function of temperature in a chosen atmosphere (5 °C/min, N_2). The ZnO–PVA mass loss curves showed that the polymer has low thermal stability, a property common to polymers of low molecular weight. The ZnO–PVA curves exhibited two specific

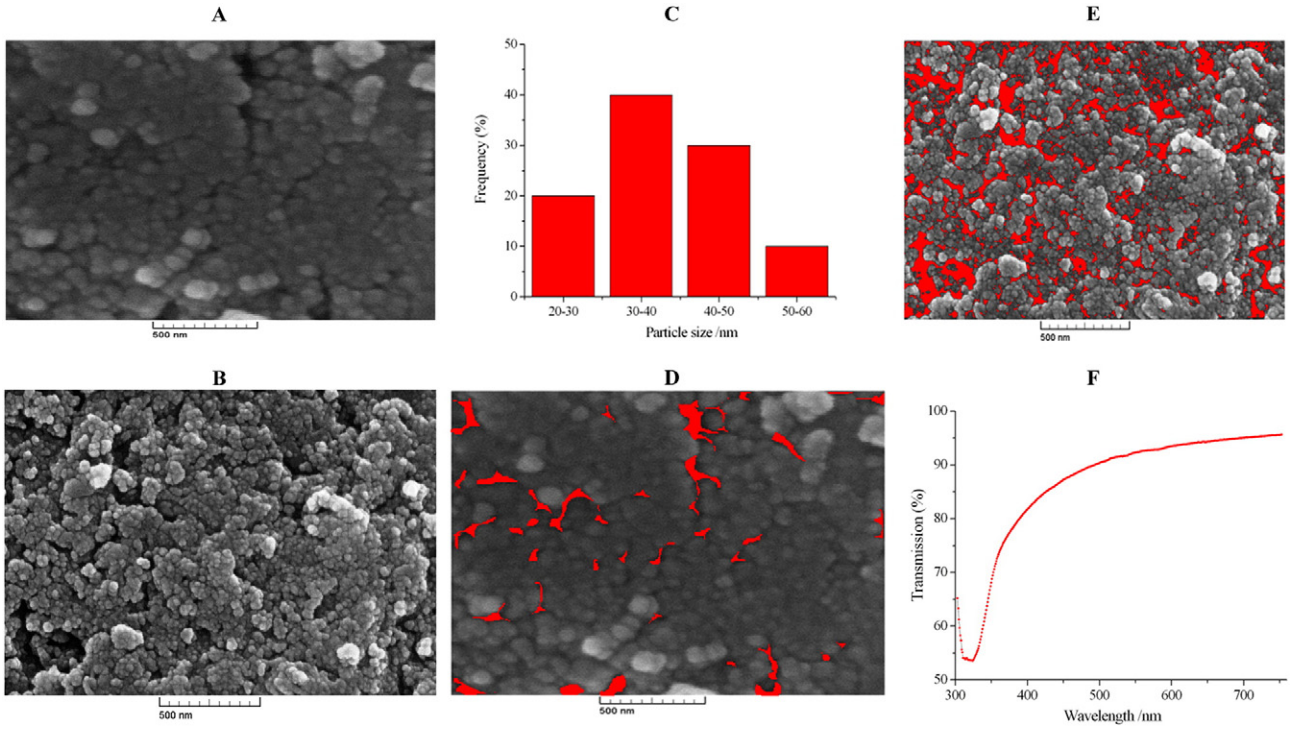

Fig. 2. FE-SEM image (A) before and (B) after annealing, (C) particle size distribution histogram, pore size distribution (D) before and (E) after annealing, and (F) UV transmission spectrum of ZnO thin film.

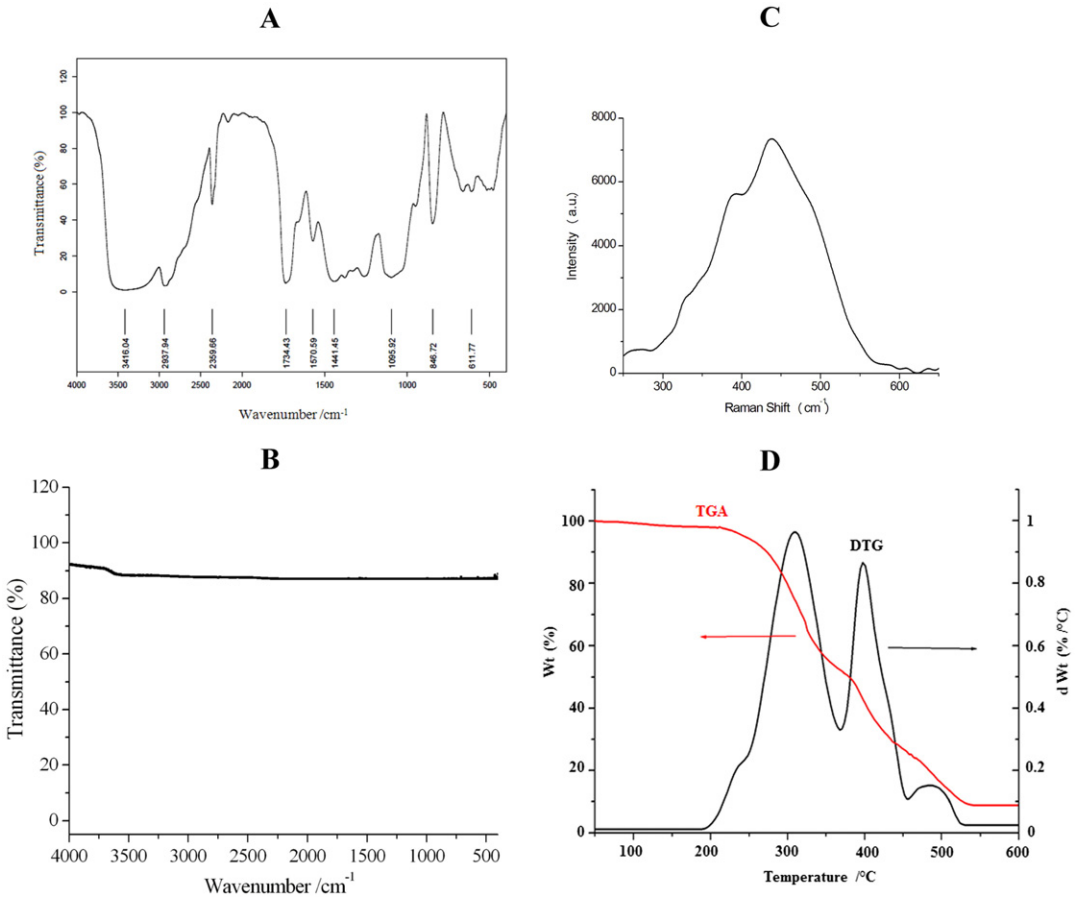

Fig. 3. (A) FTIR spectrum of ZnO–PVA nanostructured hybrid film, (B) FTIR spectrum and (C) Raman scattering spectrum of ZnO nanostructured film after annealing, and (D) TGA and DTG thermograms of ZnO–PVA.

degradation stages. The first one at 298 °C was related to the elimination of the amorphous parts of the PVA polymer while the second one, at 398 °C, corresponded to the degradation of the higher thermal stability crystalline parts (Fig. 3D). Finally, white residues (ZnO) were obtained after the TGA measurement for the ZnO–PVA hybrid [39].

3.2. Fabrication of FTO/ZnO/Urs biosensor

The primary attempt to immobilize Urs onto the FTO/ZnO electrode was through spontaneous adsorption, which occurred by electrostatic adsorption of negatively charged Urs (IEP ~ 5.9) and positively charged ZnO (IEP ~ 9.0) at a biological pH of 7.4 [40]. In addition, the optimum buffer pH for the hydrolysis of urea by Urs was considered as 7.4, at which the Urs enzyme retained its activity and natural structure required to improve detection limit and sensitivity for urea detection.

The Urs enzyme was immobilized by soaking the FTO/ZnO in a PBS, 0.1 M, pH 7.4 containing 0.2 mg mL^{-1} of Urs (100 units of Urs) for 3 h at ambient temperature [41]. The FTO/ZnO/Urs was then washed and kept in PBS until use. A step by step monitoring of the FTO/ZnO/Urs biosensor fabrication was performed using electrochemical techniques such as CV and EIS. After completing these steps, the biosensors were applied as a working electrode for urea determination using impedimetric measurements.

3.3. Determination of enzyme activity after immobilization

After Urs immobilization, the electrical property of the FTO/ZnO/Urs biosensor was studied to determine the enzyme activity. For this measurement, a cell was made, which consisted of gold wire (Φ 0.3 mm, 5 cm length) as an electrode and FTO/ZnO/Urs as another electrode. Potential range from 0.0 to 1.0 V was applied to the cell and the corresponding dc current was measured [41]. The ratio of the voltage to current was used as a measure of enzyme activity [42,43]. For each sample, five sets of measurement were carried out at the ambient temperature (25 °C). Urea solutions with various concentrations of urea such as 8, 35, 60, 85 and 110 mg dL^{-1} were prepared in PBS and used as an electrolyte. The amount of electrolyte was kept constant as 10 ml for all measurements. Since the amount of urea with respect to PBS changed with increasing urea concentration, this effect was reflected in the enzyme activity curves indicating the variation due to urea, as presented in Fig. 4. The slope of the I–V curve (ΔI/ΔV) was used as a measure of biosensor enzyme activity and was calculated using the following equation [41–43].

$$\text{Sensitivity} = \frac{(\Delta I/\Delta V)_x - (\Delta I/\Delta V)_0}{(\Delta I/\Delta V)_0} \quad (1)$$

where $(\Delta I/\Delta V)_0$ is the slope of the I–V curve at '0' mg dL^{-1} urea and $(\Delta I/\Delta V)_x$ is the slope of the I–V curve at 'x' mg dL^{-1} urea, where x = 8 to 110 mg dL^{-1} urea.

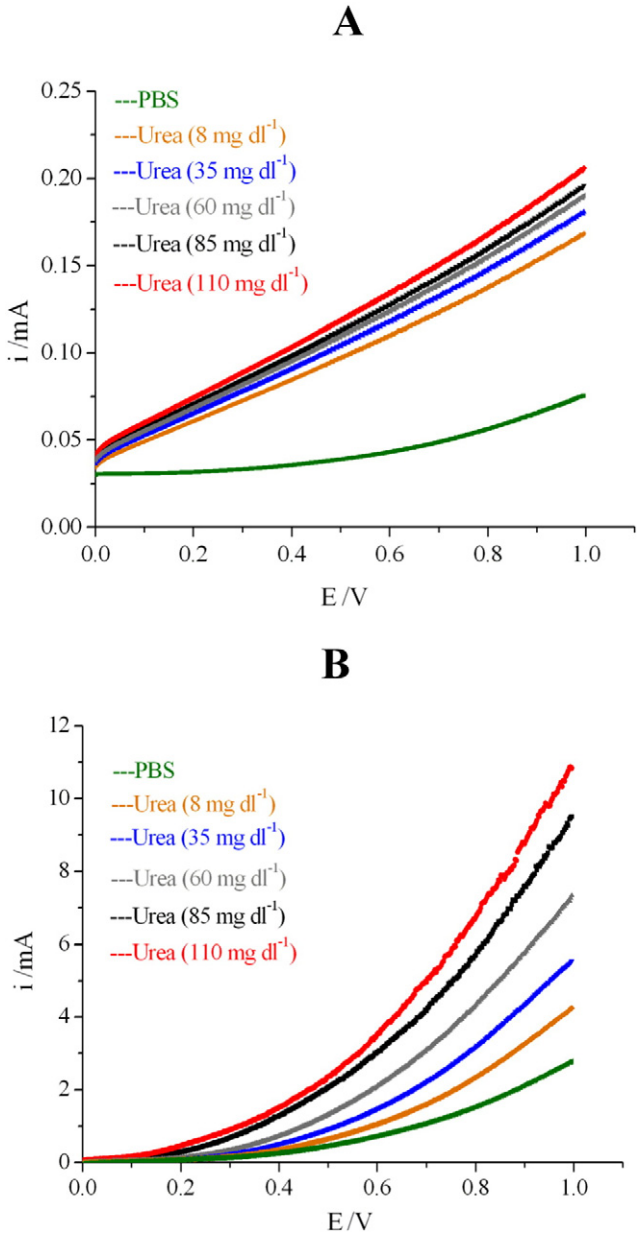

Fig. 4. Typical I–V curves showing the effect of Urs immobilization on ZnO films with increasing urea concentration, (A) before and (B) after Urs immobilization.

As can be seen in Fig. 4, it is evident that the change in response was due to the Urs immobilization. Although urea can react directly with ZnO, the Urs–urea reaction kinetics (catalytic reaction) are different than that of the ZnO–urea, therefore, the extent of the reaction may not be the same as that after the Urs immobilization. This increase was attributed to the catalytic reaction of the Urs–urea as noted below:

$$NH_2CONH_2 + 2H_2O \xrightarrow{Urs} 2NH_4^+ + CO_3^{2-}. \quad (2)$$

This reaction resulted in two NH_4^+ and CO_3^{2-} from the uncharged urea which raised the conductivity of the FTO/ZnO/Urs electrode by providing an excess electron to the conduction band. The effect of urea concentration was clearly apparent from the enzyme activity curves, so increasing enzyme activity was observed with increasing urea concentration [41–43]. The high activity of FTO/ZnO/Urs was due to the high surface area of porous ZnO film as an excellent environment for enzyme immobilization.

3.4. Impedimetric and voltammetric characterization of FTO/ZnO/Urs biosensor in the absence/presence of urea

The response of a biosensor strongly depends on the stability and performance of the enzyme, which is basically influenced by the transducer surface chemistry and immobilization strategy. Fabrication of the FTO/ZnO/Urs biosensor was studied using EIS and CV techniques. The monitoring of layer by layer assembly of the biosensor using the EIS spectrum and cyclic voltammogram was reflected by the appearance of a semicircle part corresponding to the charge transfer resistance (R_{ct}) and the magnitude of the anodic peak current (i_{pa}) of a probe

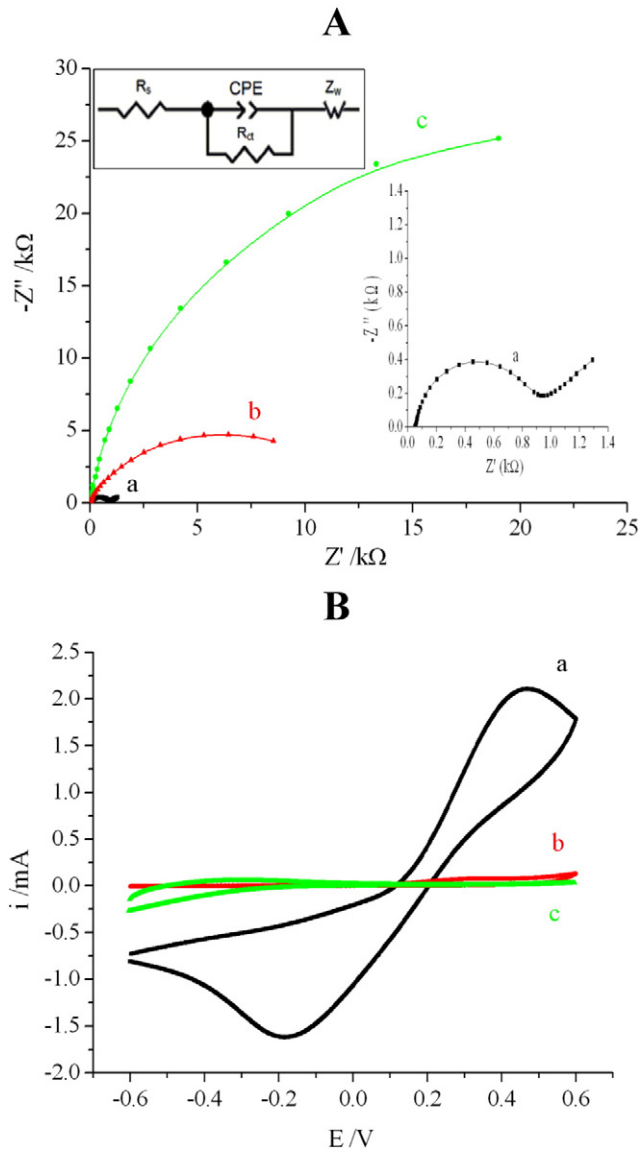

Fig. 5. (A) The Nyquist plots (–Z″ *vs.* Z′), and (B) cyclic voltammograms at the scan rate of 0.1 V s^{-1} obtained for (a) FTO, (b) FTO/ZnO, and (c) FTO/ZnO/Urs in urea-free PBS (pH 7.4) containing 5.0 mM $[Fe(CN)_6]^{3-/4-}$ as redox probe. The insets in (A) show the magnified Nyquist plot of curve a accomplished by equivalent circuit.

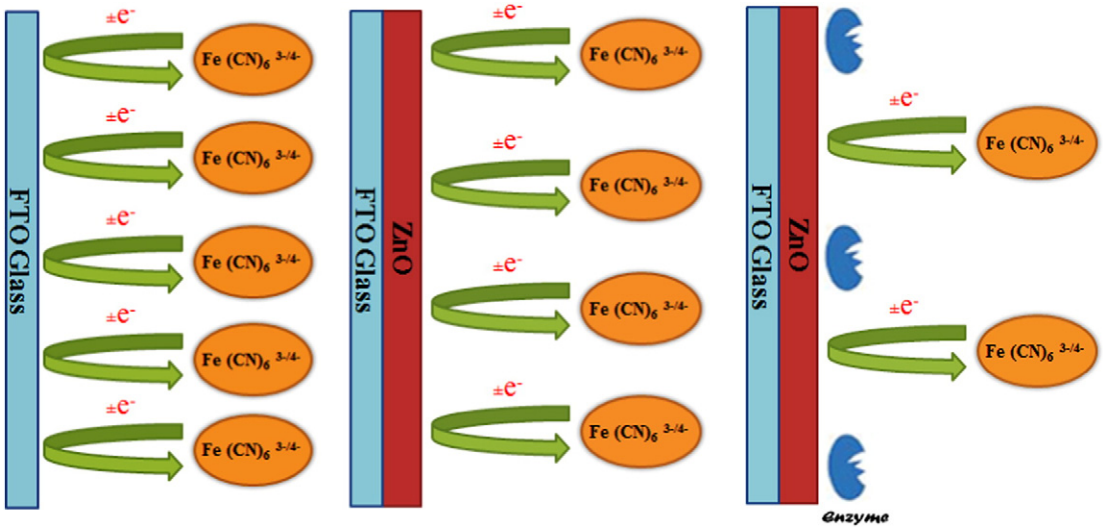

Schematic 2. The proposed mechanism for electron transfer at the FTO/ZnO/Urs electrode in the presence of $[Fe(CN)_6]^{3-/4-}$ redox probe.

($[Fe(CN)_6]^{3-/4-}$) in the urea-free electrolyte solution, respectively (Fig. 5A and B). Three layers of (a) FTO, (b) FTO/ZnO, and (c) FTO/ZnO/Urs resulted in a change of the charge transfer resistance and magnitude of the anodic peak current from (a) $R_{ct} = 0.96\ k\Omega$, $i_{pa} = 2.09$ mA to (b) $R_{ct} = 12\ k\Omega$, $i_{pa} = 0.076$ mA and (c) $R_{ct} = 60\ k\Omega$, $i_{pa} = 0.003$ mA, respectively. The R_{ct} and i_{pa} values of ZnO film (Fig. 5A and B; curve b) with respect to the FTO electrode (Fig. 5A and B; curve a) were changed, which was related to the lower electrical conductivity of the ZnO film. However, the R_{ct} value further increased and the i_{pa} value decreased (Fig. 5A and B; curve c) after the immobilization of Urs onto the FTO/ZnO electrode due to the insulating characteristics of Urs. The EIS interfacial behavior was widely described by the modified Randles equivalent circuit; in such a model, the constant phase element (CPE) is in series with the Warburg impedance (Z_w), in parallel with the charge transfer resistance (R_{ct}) and in series with the solution resistance (R_s) (Fig. 5A, inset) [41,44].

A schematic of the proposed mechanism for electron transfer at the FTO/ZnO/Urs electrode in the presence of $[Fe(CN)_6]^{3-/4-}$ redox probe is shown in Schematic 2. By comparing curves b and c in Fig. 5A and B which represent the EIS and CV spectra of $[Fe(CN)_6]^{3-/4-}$ redox reaction at FTO/ZnO and FTO/ZnO/Urs electrodes, it was observed that the Urs layer decreased direct electron transfer with electrode substrate compared with enzyme-free ZnO thin film.

The R_{ct} and i_{pa} values (Fig. 6A and B) at the interface of the FTO/ZnO/Urs biosensor in the presence of urea were obtained using EIS and CV techniques, respectively. The R_{ct} and i_{pa} values at the ZnO film ($R_{ct} = 37\ k\Omega$, $i_{pa} = 0.0147$ mA; curve b) compared with the values obtained at the FTO electrode (Fig. 6A and B; curve a) implied the partial hydrolysis of urea at the ZnO film [44]. A further decrease in R_{ct} and an increase in i_{pa} values ($R_{ct} = 19\ k\Omega$, $i_{pa} = 0.0384$ mA; curve c) were observed after the immobilization of Urs onto the FTO/ZnO substrate due to the fast hydrolysis of urea by the enzyme. The modified Randles equivalent circuit was applied for the analysis of the EIS data (Fig. 6A, inset) [41,44].

The results showed that semiconductor surfaces can be used as a base for the design of new biosensor architectures with high electron transfer facility. The electron transfer at the ZnO nanoporous surface during urea determination can be explained by the following mechanism. Initially, O_2 molecules were adsorbed on the surface of ZnO; they extracted electrons from the conduction band (E_c) of ZnO and trapped the electrons at the surface in the form of ionosorbed on the surface as O^-_{ads} (Fig. 7A). The negative charge trapped in these oxygen species caused an upward band bending and an electron depleted region, and thus a reduced conductivity (Fig. 7A).

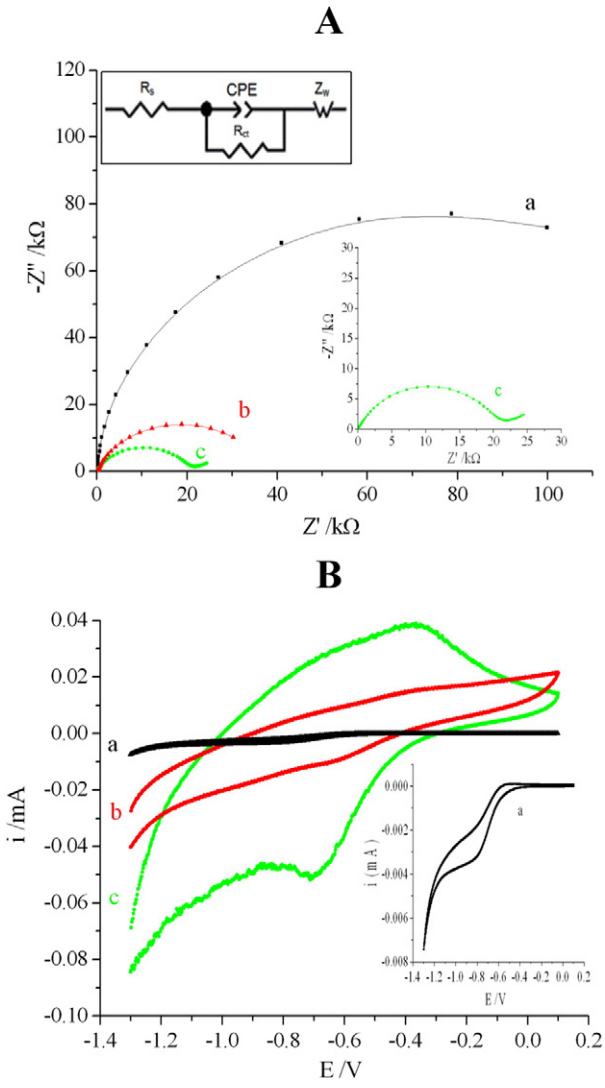

Fig. 6. (A) The Nyquist plots ($-Z''$ *vs.* Z'), and (B) cyclic voltammograms at the scan rate of 0.1 V s^{-1} obtained for (a) FTO, (b) FTO/ZnO, and (c) FTO/ZnO/Urs in PBS (pH 7.4) containing 110.0 mg dL^{-1} urea in the absence of $[Fe(CN)_6]^{3-/4-}$ probe. The insets in (A) show the magnified curve c accomplished by equivalent circuit and the inset in (B) shows the magnified curve a.

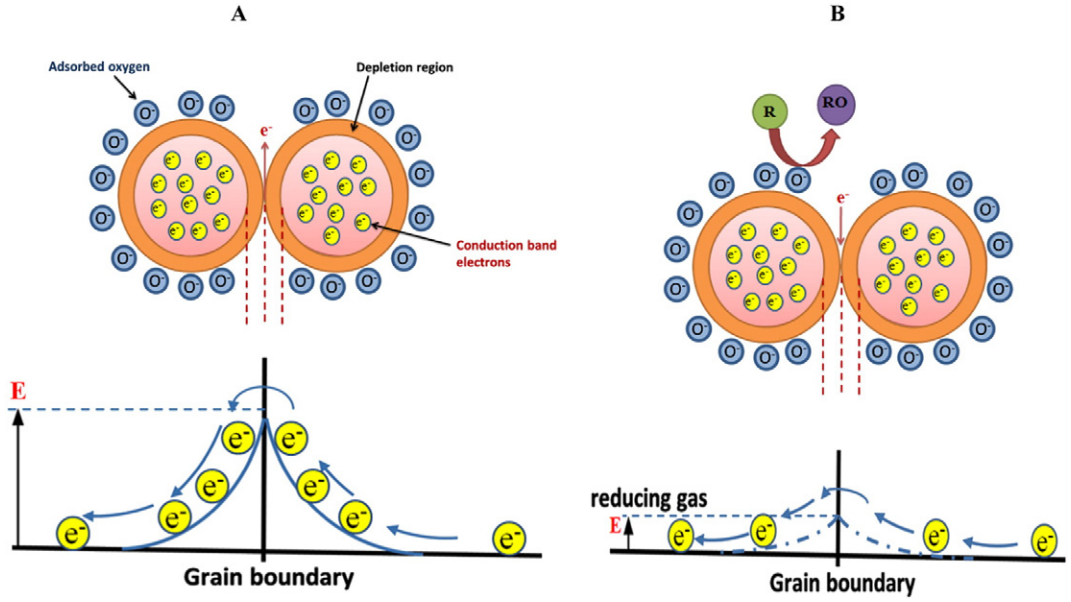

Fig. 7. The proposed mechanism of urea sensing on n-type ZnO metal oxide semiconductor in the (A) absence, and (B) presence of a reducing gas (R).

Upon exposing FTO/ZnO/Urs to urea, an enzymatic reaction took places between the Urs and the urea which can be represented as:

$$NH_2CONH_2 + 2H_2O \xrightarrow{Urs} 2NH_4^+ + CO_3^{2-}.$$

It resulted in the production of NH_4^+ ion, which reacted with the surface adsorbed oxygen (O_{ads}^-) and thereby released the trapped electron to the conduction band of ZnO as indicated by the decrease of potential barrier at the grain boundary.

$$R + O_{ads}{}^- \longrightarrow RO + e^- \quad (3)$$

Further, for n-type ZnO semiconductor, when the reducing gas (R) molecules (ammonia in the present case) react with pre-adsorbed negatively charged oxygen adsorbates, the trapped electrons were given back to the conduction band of the ZnO substrate, which reversed the band bending, and resulted in an increased conductivity (Fig. 7B) [41,44]. The results obtained by CV (Fig. 6) supported the above-mentioned sensing mechanism, which clearly points to an oxidation and reduction process.

To provide additional evidence to validate our proposed biosensing mechanism, the impedimetric response of FTO/ZnO as a function of NH_3 concentration was measured in a urea-free NH_3 solution. As shown in Fig. 8, the magnitude of R_{ct} decreased on addition of NH_3 concentration from 0.001 to 0.01 M. When reducing molecules (R = ammonia) reacted with pre-adsorbed negatively charged oxygen adsorbates (Eq. (3)), the trapped electrons were given back to the conduction band of ZnO and a decrease of R_{ct} was observed. The results obtained by the impedimetric studies of R_{ct} variation as a function of NH_3 concentration supported the proposed mechanism.

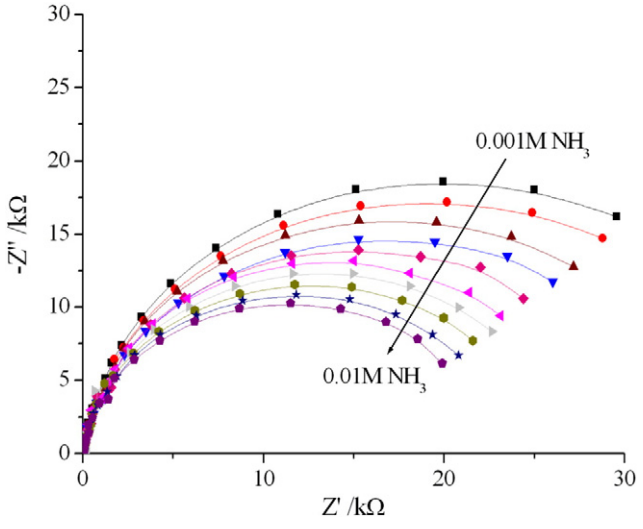

Fig. 8. The Nyquist plots (–Z″ *vs.* Z′) obtained on the FTO/ZnO electrode in the presence of different concentrations of NH_3.

3.5. Impedimetric measurements

EIS, as a powerful diagnostic tool has become increasingly popular for biosensing applications and is widely used for studying electrical and electrochemical interfacial properties of a large variety of systems. Concerning the use of EIS to study films in contact with electrolyte solutions, three different contributions, namely bulk, interfacial, and electrolytes may be determined [20–25].

The impedimetric response of the FTO/ZnO/Urs biosensor has been measured as a function of urea concentration. As shown in Fig. 9A, the magnitude of R_{ct} decreased with an increase of urea concentration from 8.0 to 110.0 mg dL^{-1} (curve a to l). Step by step impedimetric studies confirmed that the developed biosensors can be re-used (Fig. 9A). The modified Randles model was used for the approximation of EIS data for impedimetric urea detection (Fig. 9A, inset). For any fit performed, a χ^2 factor lower than 10^{-3} was obtained.

The calibration curve was obtained for urea at the FTO/ZnO/Urs biosensor by monitoring its R_{ct} responses ($|\Delta R_{ct}| = |R_{ct\ urea} - R_{ct\ buffer\ (blank)}|$). Fig. 9B displays a working curve shown in a linear scale [ΔR_{ct} (kΩ) = 5.47 (±0.04) + 0.0506 (±0.0006) [urea]; R^2 = 0.998] in a concentration range of 8.0 to 110.0 mg dL^{-1} of urea. The

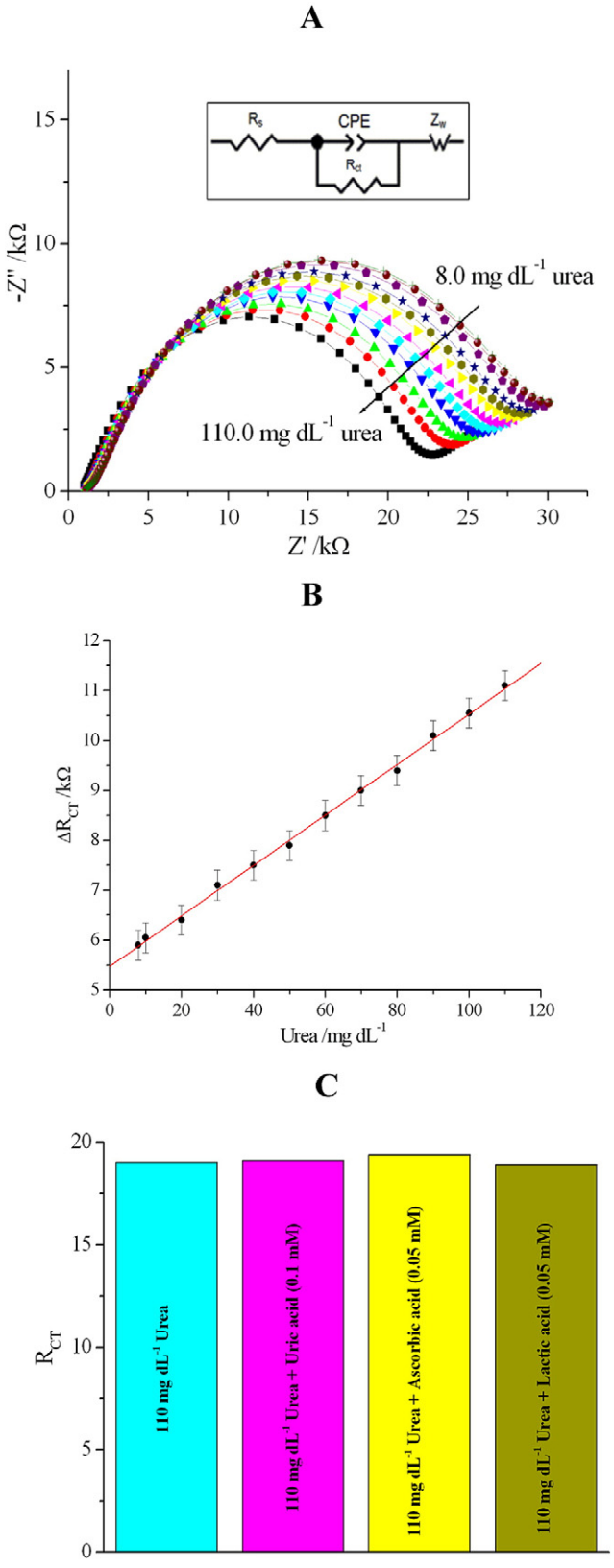

Fig. 9. (A) Nyquist plots (−Z'' *vs.* Z') obtained on the FTO/ZnO/Urs biosensor in the presence of different concentration of urea: (a) to (l) from 8.0 to 110.0 mg dL^{-1} accomplish by equivalent circuit. (B) Variation of charge transfer resistance (ΔR_{ct}) as a function of urea concentration which represents calibration curve. (C) The graph shows the effect of interferents on the response of FTO/ZnO/Urs biosensor.

Table 1
Determination of urea level in blood serum.

Method	Sample number				
	1	2	3	4	5
Determined by Spectrophotometry (mg dL^{-1})	15[b]	26.1	20.2	40[b]	17.3
Measured by FTO/ZnO/Urs (mg dL^{-1})	15.7	25.6	20.5	39.8	17.2
R.S.D.[a] (n = 5) (%)	2.19	1.21	2.16	1.05	1.10

[a] R.S.D.: Relative Standard Deviation.
[b] Represents the hyper- or hypo-level of urea in blood serum, the normal urea level in blood serum is between 15 and 40 mg dL^{-1}.

FTO/ZnO/Urs biosensor exhibited a detection limit of 5 mg dL^{-1} for urea and a sensitivity of 0.0506 kΩ per mg dL^{-1}.

Several assays were made on blood serum to test the precision of the FTO/ZnO/Urs biosensor. The urea concentration was determined by the calibration curve (Table 1). Corresponding experiments were carried out using a spectrophotometric method at a local hospital. The results exhibited good consistency and precision between the two methods and confirmed that the proposed method was useful for application in real samples providing good precision and accuracy [41,44].

The proposed FTO/ZnO/Urs biosensor had a fast response time of less than 10 s, which indicated that the structure of ZnO substrate yielded a very low mass transport barrier that resulted in a rapid diffusion from the solution toward the enzyme. The results clearly indicated that the process is a reversible process, confirming the Urs–urea enzymatic catalysis. In addition, the stability of the FTO/ZnO/Urs biosensor was tested by comparing the catalytic ability to the urea with different storage times at 4 °C. For a fixed concentration of urea, the three same biosensors lost their original activity at about 1.0%, 3.0% and 10.0% after storing times of 1 day, 2 weeks and 5 weeks, respectively. In order to study the selectivity of FTO/ZnO/Urs biosensor toward the determination of urea, EIS studies were carried out by adding normal concentration of the possible interferents present in human serum such as uric acid (0.1 mM), ascorbic acid (0.05 mM), and lactic acid (0.05 mM), separately along with the concentration of urea (110 mg dL^{-1}). The EIS analysis for all the interferents, shown in the Fig. 9C, showed a maximum interference of 2.1% with the presence of ascorbic acid. The results illustrated the importance of the prepared biosensor (FTO/ZnO/Urs) in the selective detection of urea.

Finally, based on the enzyme electrostatic immobilization strategy, the response characteristics of the FTO/ZnO/Urs biosensor with the other reported urea biosensors was compared and summarized in Table 2 [45–63]. We are currently developing nanostructured ZnO based urea biosensing using impedimetric assessment. Our results of using an electrodeposited ZnO-based urea biosensor (this work) compared with the electrostatic adsorption based biosensors (referenced in Table 2) showed adequate efficiency of the semiconductor-based biosensors with respect to the other types of used substrates. It can be postulated that the semiconductor substrate showed good linear range, low detection limit, and fast response time. The fast response time can be related to the faster electron transfer at the electrode surface as explained in the proposed mechanism.

4. Conclusions

In this study, a novel impedimetric urea biosensor was designed based on a ZnO film transducer taking many advantages including: selection of electrodeposition as a simple and controllable film preparation method, electrostatic immobilization of Urs, and impedimetric biosensing technique as a rapid assessment method. The fabricated biosensor showed high sensitivity, low detection limit, broad dynamic

Table 2
Analytical characteristics of FTO/ZnO/Urs biosensor compared with the values of other reported urea biosensors based on Urs physical immobilization strategy.

Matrix	Response characteristics			Stability (life time)	Detection method	Ref
	DR (mg dL^{-1})	DL (mg dL^{-1})	RT			
Whatman paper	10–99 mg dL^{-1}	10 mg dL^{-1}	2 min	–	Potentiometric	[45]
Polyaniline–poly(n-butylmethacrylate)	20–120 mg dL^{-1}	20 mg dL^{-1}	10 min	–	Conductometric	[46]
Nano-porous silicon	10–100 mmol L^{-1}	–	<1 min	–	Amperometric	[47]
Gold-coated plastic substrates	0.1–100 mM	0.1 mM	4 s	3 weeks	Potentiometric	[48]
Polyaniline	10^{-6}–10^{-1} mol L^{-1}	–	–	3 weeks	Potentiometric	[49]
Graphite and platinum composite electrode	10–250 μM	3 μM	2 min	3 months	Amperometric	[50]
Carboxylic poly(vinylchloride)	10^{-5}–10^{-1} M	0.28 mM	–	–	Potentiometric	[51]
Electropolymerized toluidine blue film	0.2–0.8 mM	0.2 mM	20–30 s	1 day	Amperometric	[17]
Polyethylenimine	$10^{-2.5}$–$10^{-1.5}$ M	$10^{-2.5}$ M	15–30 s	4 weeks	Potentiometric	[52]
Nanoporous Alumina	0.5 μM–3.0 mM	0.2 μM	30 s	1 month	Conductometric	[53]
Tetramethylorthosilicate (TMOS)	0.01–30 mM	52 μg mL^{-1}	–	25 days	Potentiometric	[54]
Laser ablated ZnO thin film	5–200 mg dL^{-1}	–	–	12 weeks	Amperometric	[55]
ZnO nanoparticles	10–80 mg dL^{-1}	13.5 mg dL^{-1}	–	3 weeks	Cyclic Voltammetry	[56]
Cs–Co_3O_4 nanocomposite	10^{-4}–8×10^{-2} M	–	12 s	2 weeks	Potentiometric	[57]
NiO nanoparticles	0.83–16.65 mM	21.3 μA	5 s	20 weeks	Cyclic Voltammetry	[58]
Zinc oxide-chitosan	5–100 mg dL^{-1}	3 mg dL^{-1}	10 s	3 months	Cyclic Voltammetry	[14]
Mn^{2+} doping in TiO_2 thin films	0–6.5 mg mL^{-1}	–	–	–	Chronoamperometry	[59]
Silicalite	5–850 μM	–	3 min	10 days	Conductometric	[60]
BSA embedded surface modified polypyrrole film	6.6×10^{-6}–7.5×10^{-4} M	–	70–90 s	2 months	Potentiometric	[61]
TiO_2 film	8 μM–3 mM	5 μM	25 s	1 month	Potentiometric	[62]
ZnO nanorods	0.001–24.0 mM	10 μM	–	20 weeks	Cyclic Voltammetry	[63]
Sputtered ZnO thin film	5–140 mg dL^{-1}	2.42 mg dL^{-1}	4 s	3 weeks	Impedimetric	[41]
Electrodeposited nanoporous ZnO	8–110 mg dL^{-1}	5 mg dL^{-1}	10 s	3 weeks	Impedimetric	This work

Detection Range [DR], Detection Limit [DL], Response Time [RT].

range, and a fast response time. The impedimetric analysis of the proposed biosensor indicated a fast response time of less than 10 s with a wide linear range from 8.0 to 110.0 mg dL^{-1} and the limit of detection as 5.0 mg dL^{-1} for urea.

Acknowledgment

S. A. Mozaffari acknowledges the support rendered by the Iranian Research Organization for Science and Technology (IROST), and Iran Nanotechnology Initiative Council (INIC).

References

[1] M. Singh, N. Verma, A.K. Garg, N. Redhu, Urea biosensors, Sensors Actuators B Chem. 134 (2008) 345.
[2] G.P. Nikoleli, D.P. Nikolelis, C. Methenitis, Construction of a simple optical sensor based on air stable lipid film with incorporated urease for the rapid detection of urea in milk, Anal. Chim. Acta 675 (2010) 58.
[3] H.C. Tsai, R.A. Doong, Simultaneous determination of pH, urea, acetylcholine and heavy metals using array-based enzymatic optical biosensor, Biosens. Bioelectron. 20 (2005) 1796.
[4] B. Kovacs, G. Nagy, R. Dombi, K. Toth, Optical biosensor for urea with improved response time, Biosens. Bioelectron. 18 (2003) 111.
[5] R. Ramesh, P. Puhazhendi, J. Kumar, M. Gowthaman, S. D'Souza, N. Kamini, Potentiometric biosensor for determination of urea in milk using immobilized arthrobacter creatinolyticus urease, Mater. Sci. Eng. C Mater. Biol. Appl. 49 (2015) 786.
[6] A. Ali, M. AlSalhi, M. Atif, A.A. Ansari, M.Q. Israr, J. Sadaf, E. Ahmed, O. Nur, M. Willander, Potentiometric urea biosensor utilizing nanobiocomposite of chitosan-iron oxide magnetic nanoparticles, Journal of Physics: Conference SeriesIOP Publishing 2013, p. 012024.
[7] D. Chirizzi, C. Malitesta, Potentiometric urea biosensor based on urease immobilized by an electrosynthesized poly(o-phenylenediamine) film with buffering capability, Sensors Actuators B Chem. 157 (2011) 211.
[8] K. Saeedfar, L. Heng, T. Ling, M. Rezayi, Potentiometric urea biosensor based on an immobilised fullerene–urease bio-conjugate, Sensors (2013) 16851.
[9] O.Y. Saiapina, V.M. Pyeshkova, O.O. Soldatkin, V.G. Melnik, B.A. Kurc, A. Walcarius, S.V. Dzyadevych, N. Jaffrezic-Renault, Conductometric enzyme biosensors based on natural zeolite clinoptilolite for urea determination, Mater. Sci. Eng. C 31 (2011) 1490.
[10] S.K. Kirdeciler, E. Soy, S. Ozturk, I. Kucherenko, O. Soldatkin, S. Dzyadevych, B. Akata, A novel urea conductometric biosensor based on zeolite immobilized urease, Talanta 85 (2011) 1435.
[11] W.Y. Lee, S.R. Kim, T.H. Kim, K.S. Lee, M.C. Shin, J.K. Park, Sol–gel-derived thick-film conductometric biosensor for urea determination in serum, Anal. Chim. Acta 404 (2000) 195.
[12] J. Kato, T. Koseki, Y. Aoki, A. Yamada, T. Tanaka, Coulometric titration of urea with electrogenerated hypobromite, Anal. Sci. 29 (2013) 753.
[13] I. Bozgeyik, M. Senel, E. Cevik, M.F. Abasiyanik, A novel thin film amperometric urea biosensor based on urease-immobilized on poly(N-glycidylpyrrole-co-pyrrole), Curr. Appl. Phys. 11 (2011) 1083.
[14] P.R. Solanki, A. Kaushik, A.A. Ansari, G. Sumana, B.D. Malhotra, Zinc oxide-chitosan nanobiocomposite for urea sensor, Appl. Phys. Lett. 93 (2008) 163903.
[15] A.P. Soldatkin, J. Montoriol, W. Sant, C. Martelet, N. Jaffrezic-Renault, A novel urea sensitive biosensor with extended dynamic range based on recombinant urease and ISFETs, Biosens. Bioelectron. 19 (2003) 131.
[16] G.P. Nikoleli, M.Q. Israr, N. Tzamtzis, D.P. Nikolelis, M. Willander, N. Psaroudakis, Structural characterization of graphene nanosheets for miniaturization of potentiometric urea lipid film based biosensors, Electroanalysis 24 (2012) 1285.
[17] I. Vostiar, J. Tkac, E. Sturdik, P. Gemeiner, Amperometric urea biosensor based on urease and electropolymerized toluidine blue dye as a pH-sensitive redox probe, Bioelectrochemistry 56 (2002) 113.
[18] M.H. Keyes, R. Barabino, Development of immobilized urease for the Owens-Illinois bun analyzer, Enzym. Eng. 1 (1978) 51.
[19] R.E. Adams, P.W. Carr, Coulometric flow analyzer for use with immobilized enzyme reactors, Anal. Chem. 50 (1978) 944.
[20] S.A. Mozaffari, M. Saeidi, R. Rahmanian, Photoelectric characterization of fabricated dye-sensitized solar cell using dye extracted from red Siahkooti fruit as natural sensitizer, Spectrochim. Acta A 142 (2015) 226.
[21] S.A. Mozaffari, M. Ranjbar, E. Kouhestanian, H. Salar Amoli, M.H. Armanmehr, An investigation on the effect of electrodeposited nanostructured ZnO on the electron transfer process efficiency of TiO_2 based DSSC, Mater. Sci. Semicond. Process. 40 (2015) 285.
[22] R. Shabani, S.A. Mozaffari, S. Waqif Husain, M. Saber Tehrani, Selective nanosensing of copper (II) ion using L-Lysine in-situ functionalized gold cysteamine self-assembled monolayer, Iran. J. Sci. Technol. 33 (2009) 335.
[23] R.K. Shervedani, S.A. Mozaffari, Copper (II) nanosensor based on a gold cysteamine self-assembled monolayer functionalized with salicylaldehyde, Anal. Chem. 78 (2006) 4957.
[24] S.A. Mozaffari, T. Chang, S.M. Park, Diffusional electrochemistry of cytochrome c on mixed captopril/3-mercapto-1-propanol self-assembled monolayer modified gold electrodes, J. Phys. Chem. C 113 (2009) 12434.
[25] S.A. Mozaffari, T. Chang, S.M. Park, Self-assembled monolayer as a pre-concentrating receptor for selective serotonin sensing, Biosens. Bioelectron. 26 (2010) 74.
[26] M.P. Massafera, S.I.C. Torresi, Urea amperometric biosensors based on a multifunctional bipolymeric layer: comparing enzyme immobilization methods, Sensors Actuators B Chem. 137 (2009) 476.
[27] Z. Chen, Y. Tang, L. Zhang, L. Luo, Electrodeposited nanoporous ZnO films exhibiting enhanced performance in dye-sensitized solar cells, Electrochim. Acta 51 (2006) 5870.
[28] S.A. Kamaruddin, K.Y. Chan, M.Z. Sahdan, M. Rusop, H. Saim, ZnO microstructures and nanostructures prepared by sol–gel hydrothermal technique, J. Nanosci. Nanotechnol. 10 (2010) 5618.
[29] L. Miao, S. Cai, Z. Xiao, Preparation and characterization of nanostructured ZnO thin film by electrophoretic deposition from ZnO colloidal suspensions, J. Alloys Compd. 490 (2010) 422.
[30] H.S. Al-Salman, M.J. Abdullah, Hydrogen gas sensing based on ZnO nanostructure prepared by RF-sputtering on quartz and PET substrates, Sensors Actuators B Chem. 181 (2013) 259.

[31] N.J. Ridha, A.A. Umar, F. Alosfur, M.H. Jumali, M.M. Salleh, Microwave assisted hydrothermal method for porous zinc oxide nanostructured-films, J. Nanosci. Nanotechnol. 13 (2013) 2667.
[32] Q. Humayun, M. Kashif, U. Hashim, Area-selective ZnO thin film deposition on variable microgap electrodes and their impact on UV sensing, J. Nanomater. 2013 (2013) 1.
[33] T. Pauporte, Highly transparent ZnO/Polyvinyl alcohol hybrid films with controlled crystallographic orientation growth, Cryst. Growth Des. 7 (2007) 2310.
[34] J.R. Macdonald, J. Schoonman, A.P. Lehnen, Applicability and power of complex nonlinear least squares for the analysis of impedance and admittance data, J. Electroanal. Chem. 131 (1982) 77.
[35] B. Arifvianto, J. Zhou, Fabrication of metallic biomedical scaffolds with the space holder method: a review, Materials 7 (2014) 3588.
[36] L. Vayssieres, On Solar Hydrogen and Nanotechnology, first ed. Wiley, Asia, 2010.
[37] A. Kumar, Nanofibers, first ed. InTech, Asia, 2010.
[38] Y. Dong, C. Feng, P. Jiang, G. Wang, K. Li, H. Miao, Simple one-pot synthesis of ZnO/Ag heterostructures and the application in visible-light-responsive photocatalysis, RSC Adv. 4 (2014) 7340.
[39] K. Dassios, Poly (vinyl alcohol)-infiltrated carbon nanotube carpets, Mater. Sci. Appl. 3 (2012) 658.
[40] P. Netzahualcoyotl, B. Marcia, A. Sunil, H. Samuel, T. Maharaj, R. Jaime, S. Surinder, Zinc oxide nanorods modified indium tin oxide surface for amperometric urea biosensor, J. Nanosci. Nanotechnol. 11 (2011) 6683.
[41] S.A. Mozaffari, R. Rahmanian, M. Abedi, H.S. Amoli, Urea impedimetric biosensor based on reactive RF magnetron sputtered zinc oxide nanoporous transducer, Electrochim. Acta 146 (2014) 538.
[42] S.G. Ansari, Z.A. Ansari, R. Wahab, Y. Kim, G. Khang, H. Shin, Glucose sensor based on nano-baskets of tin oxide templated in porous alumina by plasma enhanced CVD, Biosens. Bioelectron. 23 (2008) 1838.
[43] S. Mahadeva, J. Kim, Conductometric glucose biosensor made with cellulose and tin oxide hybrid nanocomposite, Sensors Actuators B Chem. 157 (2011) 177.
[44] R. Rahmanian, S.A. Mozaffari, Electrochemical fabrication of ZnO-polyvinyl alcohol nanostructured hybrid film for application to urea biosensor, Sensors Actuators B Chem. 207 (2015) 772.
[45] N. Verma, M. Singh, A disposable microbial based biosensor for quality control in milk, Biosens. Bioelectron. 18 (2003) 1219.
[46] M.M. Castillo-Ortega, D.E. Rodriguez, J.C. Encinas, M. Plascencia, F.A. Mendez-Velarde, R. Olayo, Conductometric uric acid and urea biosensor prepared from electroconductive polyaniline-poly (n-butyl methacrylate) composites, Sensors Actuators B Chem. 85 (2002) 19.
[47] J.H. Jin, S.H. Paek, C.W. Lee, N.K. Min, S.I. Hong, Fabrication of amperometric urea sensor based on nano-porous silicon technology, J. Korean Phys. Soc. 42 (2003) 735.
[48] S.M.U. Ali, Z.H. Ibupoto, S. Salman, O. Nur, M. Willander, B. Danielsson, Selective determination of urea using urease immobilized on ZnO nanowires, Sensors Actuators B Chem. 160 (2011) 637.
[49] B. Lakard, D. Magnin, O. Deschaume, G. Vanlancker, K. Glinel, S. Demoustier-Champagne, B. Nysten, A.M. Jonas, P. Bertrand, S. Yunus, Urea potentiometric enzymatic biosensor based on charged biopolymers and electrodeposited polyaniline, Biosens. Bioelectron. 26 (2011) 4139.
[50] A. Pizzariello, M. Stredansky, S. Stredanska, S. Miertus, Urea biosensor based on amperometric pH-sensing with hematein as a pH-sensitive redox mediator, Talanta 54 (2001) 763.
[51] Z. Wu, L. Guan, G. Shen, R. Yu, Renewable urea sensor based on a self-assembled polyelectrolyte layer, Analyst 127 (2002) 391.
[52] B. Lakard, G. Herlem, S. Lakard, A. Antoneou, B. Fahys, Urea potentiometric biosensor based on modified electrodes with urease immobilized on polyethylenimine films, Biosens. Bioelectron. 19 (2004) 1641.
[53] Y. Zhengpeng, S. Shihui, D. Hongjuan, Z. Chunjing, Piezoelectric urea biosensor based on immobilization of urease onto nanoporous alumina membranes, Biosens. Bioelectron. 22 (2007) 3283.
[54] R. Sahney, S. Anand, B. Puri, A. Srivastava, A comparative study of immobilization techniques for urease on glass-pH-electrode and its application in urea detection in blood serum, Anal. Chim. Acta 578 (2006) 156.
[55] N. Batra, M. Tomar, P. Jain, V. Gupta, Laser ablated ZnO thin film for amperometric detection of urea, J. Appl. Phys. 114 (2013) 124702.
[56] A. Ali, A.A. Ansari, A. Kaushik, P.R. Solanki, A. Barik, M.K. Pandey, B.D. Malhotra, Nanostructured zinc oxide film for urea sensor, Mater. Lett. 63 (2009) 2473.
[57] A. Ali, M. Israr-Qadir, Z. Wazir, M. Tufail, Z. Ibupoto, S. Jamil-Rana, M. Atif, S. Khan, M. Willander, Cobalt oxide magnetic nanoparticles-chitosan nanocomposite based electrochemical urea biosensor, Indian J. Phys. 1 (2014) 1.
[58] M. Tyagi, M. Tomar, V. Gupta, NiO nanoparticle-based urea biosensor, Biosens. Bioelectron. 41 (2013) 110.
[59] D. Marshal, Using nano-arrayed structures in sol–gel derived Mn^{2+} doped TiO_2 for high sensitivity urea biosensor, J. Biosens. Bioelectron. 1 (2010) 1.
[60] I. Kucherenko, O. Soldatkin, B.O. Kasap, S. Öztürk, B. Akata, A. Soldatkin, S. Dzyadevych, Elaboration of urease adsorption on silicalite for biosensor creation, Electroanalysis 24 (2012) 1380.
[61] T. Ahuja, I.A. Mir, D. Kumar, Potentiometric urea biosensor based on BSA embedded surface modified polypyrrole film, Sensors Actuators B Chem. 134 (2008) 140.
[62] X. Chen, Z. Yang, S. Si, Potentiometric urea biosensor based on immobilization of urease onto molecularly imprinted TiO_2 film, J. Electroanal. Chem. 635 (2009) 1.
[63] R. Ahmad, N. Tripathy, Y.B. Hahn, Highly stable urea sensor based on ZnO nanorods directly grown on Ag/glass electrodes, Sensors Actuators B Chem. 194 (2014) 290.